Journal of Surface Engineered Materials and Advanced Technology, 2022, 12, 35-59
https://www.scirp.org/journal/jsemat
ISSN Online: 2161-489X
ISSN Print: 2161-4881

Musa Paradaisica and *Vitis vinifera* Functionalised Ag-NPs: Electrochemical and Optical Detection of *Escherichia coli* in Seawater

Sphamandla Nqunqa[1], Takalani Mulaudzi[2], Njagi Njomo[3], Usisipho Feleni[4], Rachel F. Ajayi[1*]

[1]SensorLab, Chemistry Department, Chemical Sciences Building, University of the Western Cape, Bellville, South Africa
[2]Biotechnology Department, Life Sciences Building, University of the Western Cape, Bellville, South Africa
[3]Chemistry Department, Riverside Drive off, University of Nairobi, Waiyaki Way, Nairobi, Kenya
[4]Institute for Nanotechnology and Water Sustainability (iNanoWS), College of Science, Engineering and Technology, University of South Africa, Florida Campus Roodepoort, South Africa
Email: *fngece@uwc.ac.za

How to cite this paper: Nqunqa, S., Mulaudzi, T., Njomo, N., Feleni, U. and Ajayi, R.F. (2022) Musa Paradaisica and *Vitis vinifera* Functionalised Ag-NPs: Electrochemical and Optical Detection of *Escherichia coli* in Seawater. *Journal of Surface Engineered Materials and Advanced Technology*, **12**, 35-59.
https://doi.org/10.4236/jsemat.2022.123004

Received: July 1, 2022
Accepted: July 26, 2022
Published: July 29, 2022

Abstract

Herein, we demonstrate a simple and inexpensive one-pot green synthesis of silver nanoparticles (Ag-NPs) functionalised with a combination of banana peel (*Musa paradisiaca)* and grape (*Vitis vinifera*) fruit extracts. The reaction mixture of aqueous silver nitrate, banana peel and grapefruit extracts revealed a dark brown colour after a reaction time of 18 minutes, which indicates the presence and the successful synthesis of silver nanoparticles. The optical and structural properties of the green synthesised nanoparticles were analysed using UV-Visible spectroscopy (UV-Vis) which confirmed an absorption band at 440 nm. The polydispersity nature and the AgNPs sizes of 30 nm were revealed using small angle X-ray scattering (SAXS) and high-resolution transmission electron microscopy (HR-TEM) techniques. Fourier transform infrared spectroscopy (FT-IR) studies revealed the structure of these nanoparticles which included carbonyl groups, primary amine groups, OH groups and other stabilizing functional groups characteristic of the properties of combined extracts. A simple, quick, less time-consuming surface plasmon resonance (SPR) and electrochemical method in the form of optical and electrochemical sensors have been developed for the detection of *Escherichia coli* 0157:H7. The obtained limit of detection (LOD) values for SPR and GBPE-Ag-NPs/GCE-based sensor systems were found to be 1 × 102 CFU/mL and 3.5 × 101 CFU/mL, respectively. The obtained values fall within the range for *E. coli* 0157:H7 in seawater.

Keywords

Cyclic Voltammetry, Electrochemical Sensors, *Escherichia coli* 0157:H7, *Musa paradisiaca*, *Vitis vinifera*, Silver Nanoparticles

1. Introduction

Contaminated seawater is a health hazard which, in some cases, leads to fatality. Swimmers and surfers swallow significant amounts of water whereas adult swimmers are prone to ingest between 10 and 100 ml of seawater, while children probably consume more massive quantities of water. The highest risk lies primarily with young children, grown-ups and people infected with Human Immune Virus (HIV) and Tuberculosis (TB) who are at risk to suffer health hazards by ingesting sewage polluted seawater. Therefore, they need to be informed about the risk and health hazards of diseases such as skin infection, diarrhea, respiratory tract infection, and hepatitis which they can easily contract by swimming in contaminated seawater [1]. Human waterborne diseases result from exposure to water that is contaminated or untreated [2]. According to the World Health Organization (WHO), pathogen contamination is a significant issue throughout the world [2]. Furthermore, health protection programs in South Africa also reveal studies giving evidence of the presence of high levels of contamination in seawater by micro-organisms [2]. The bacteriological control of water quality requires the quantification and detection of faecal contamination indicators to signal the presence of potentially harmful pathogens of faecal origin such as *E. coli* and other pathogens [3].

The presence of *Escherichia coli* (*E. coli*) in the water source or water supply indicates faecal contamination and it is now recognised in South Africa as the most fatal by the Department of Environmental Affairs (DEA). *Escherichia coli* is a gram-negative, rod-shaped bacterium and it is well known as *E. coli.* This bacterium is usually in the lowest guts of warm-blooded animals or the intestines; it may also be found in the guts of human beings [4]. This type of bacterium may or may not be mobile since some of them have flagellated rods, and some are not. Some strains of *E. coli* are harmless, but there is one dangerous strain called *E. coli* 0157:H7 [5]. *E. coli* 0157:H7 strain is well known as the most aggressive strain among hundreds of bacteria, due to its ability to produce a dominant toxin known as Shiga toxin that can cause diarrhea, kidney failure, hemolytic uremic syndrome or death. *E. coli* 0157:H7 bacteria were recognized in 1982 for the first time as a cause of illness during an outbreak which caused bloody diarrhea in people who drank contaminated water [6]. According to the report made by Tam and co-workers, 600 million cases of human diarrhea and 800,000 worldwide deaths mainly in children under the age of 5 years were due to *E. coli* 0157:H7 [7]. According to WHO and national standards when viable cell numbers of *E. coli* in water range between 100 - 1000 CFU/mL, the water is

considered to be at intermediate risk and high risk is declared when the *E. coli* cells range between 100 - 1000 CFU/mL. However, the South African National Standards (SANS) declare drinking water to be safe only when there are no cells of *E. coli* detected [8]. The presence of micro-organisms such as *E. coli*, Mycobacterium avium, Listeria monocytogenes, salmonella and viruses like Noro-virus, Hepatitis A and others in freshwater or seawater indicate a sign of pollution [9] and possess a significant risk to human health. Previous reports on the microbiological quality of South African rivers showed that the water source was unsafe for human consumption in some areas. Furthermore, they report that *E. coli* was one of the primary potential pathogens found [10].

The current conventional methods for monitoring recreational beach waters for faecal indicator bacteria are performed using culture-based technologies, Plate Count Enumeration Method and Membrane Filter (MF) technique [11], and Multiple Tube Fermentation (MTF) [12]. Colony counting and culture-based methods [13] enzyme-linked immunosorbent assay [14] and polymerase chain reaction (PCR) [15] require more than a day for laboratory analysis. During this time, swimmers are at risk. Other drawbacks of these methods are the use of toxic substances and are high cost. Therefore, rapid methods for detecting and counting *E. coli* in recreational waters (seawater and freshwater) must be designed and implemented to predict any contamination better and to allow for improved water quality management [16] [17]. These methods need to be more effective with much less toxicity and the promising alternatives include the use of metal and metal oxide nanoparticles which have had substantial results. Exploration of nanobiotechnology through the application of materials like nanoparticles such as silver nanoparticles is worth investigating in order to gain insight into alternative local and possibly systemic antibacterial therapeutic elements.

Green synthetic routes have several merits such as their simplicity, low cost, non-toxic products and stable nanoparticles [18]. In the field of nanomaterials, silver nanoparticles (Ag-NPs) have attracted considerable attention due to their biocompatibility, stability and oxidation resistance. Additionally, they have also found applications in sensing, imaging, electronics, catalysis and biomedicine where their catalytic and physiochemical properties are governed by their crystal structure, shape and size [19]. In a majority of studies, Ag-NPs have been shown to be synthesized using reducing agents such as citrates, hydrazine and borohydride and modified with appropriate capping ligands. These conventional protocols for the fabrication of Ag-NPs have also shown to involve expensive techniques, inefficient energy consumption and the use of toxic chemicals. Consequently, due to the increase in demand for the development of nanomaterials across a widespread of applications, this may result in unintended harmful exposure to human beings especially in the field of nanomedicine Hence, a necessary step to ensure a sustainable future is imperative and can be achieved through the use of biological systems such as microorganisms and plant extracts [20]. As such, the synthesis of nanoparticles using fruit extracts has been reported to be cost-effective and much simpler

since it involves single-step procedures. In Sub-Saharan Africa, grapes and bananas are well-known fruits that are harvested by small and large producers. The amount of production of these fruits is estimated to be more than 72 million worldwide [21]. Moreover, the high level of production of these two fruits is due to their beneficial effects on human health [22]. Different parts of their fruit material such as seeds [23] stalks and peels have been reported in the literature for the synthesis of different sized and shaped nanoparticles [24].

Therefore, for the first time, this research presents the use of a mixture of *Musa paradaisica* peels and *Vitis vinifera* fruit extracts to synthesise silver nanoparticles without using any form of external chemical stabilizing or reducing agents. The sensor development potential of these nanoparticles was also explored through electrochemical and surface plasmon resonance analyses as a sensing platform for seawater monitoring of *E. coli* 0157:H7.

2. Materials and Methods

2.1. Reagents and Materials

Silver nitrate ($AgNO_3$, 99.9%) was used in the synthesis of the nanoparticles and the electrolyte used throughout this study was pH 7.4, 0.2 M phosphate buffer (PBS). PBS was prepared using sodium phosphate monobasic dihydrate ($NaH_2PO_4{\cdot}2H_2O$, 99%) and sodium phosphate dibasic dihydrate ($Na_2HPO_4{\cdot}2H_2O$, 99.5%). All were purchased from Sigma Aldrich, Kempton Park, Johannesburg, South Africa. Fresh bananas and grapes used as capping and stabilizing agents in the synthesis of the nanoparticles were purchased from Checkers Hypermarket, Cape Town, South Africa. The deionised ultra-purified water prepared with a Milli-Q water purification system was procured from Merck KGaA, Darmstadt, Germany. When not in use, the prepared electrolyte solutions were kept refrigerated at 4˚C.

2.2. Instrumentation

High-Resolution Transmission Electron Microscopic (HR-TEM) analyses of the nanoparticles were performed with a Tecnai G2 F20 X-Twin HRTEM purchased from FEI Company, Hillsboro, OR, United States of America. Cyclic Voltammetry (CV) studies were performed with a PalmSens3 Potentiostat from PalmSens3 BV, Houten, The Netherlands. Furthermore, the structural and optical properties of the synthesised silver nanoparticles were studied with Ultraviolet-Visible (UV-Vis) Spectroscopy (with a Nicolett Evolution 100 from Thermo Electron Corporation, Johannesburg, South Africa) and Fourier Transform Infrared Spectroscopy (FT-IR) using a PerkinElmer Spectrum 100-FT-IR Spectrometer from PerkinElmer (Pty) Ltd., Midrand, South Africa. The internal structure of the nanoparticles was studied with Small-Angle X-ray Scattering (SAXS) (Anton Paar, GmbH, Australia).

2.3. Synthesis of Silver Nanoparticles (Ag-NPs)

Banana peels were separated from bananas and then finely cut before being

washed repeatedly together with 50 g grapes using ultra-purified water to remove any dust and organic impurities. Thereafter, the grapes and cut banana peels were placed into different beakers containing 300 mL distilled water where each mixture was heated at 80˚C and stirred at 1000 rpm for 30 min. The extracts were then kept at room temperature and allowed to cool followed by centrifugation at 1000 rpm for 30 min. The obtained products were filtered twice to remove any insoluble fractions and macromolecules. The two extracts were then combined at various ratios, however, the ratio of 1 (banana):3 (grape) was found to synthesize the most stable nanoparticles with shelf-lives in excess of 3 months.

In this study, the natural reducing agents present in grapes and banana peels were used to produce silver nanoparticles. A stock solution of 2.0×10^{-5} M $AgNO_3$ was prepared in 100 mL ethanol. Then, 50 mL of the $AgNO_3$ stock solution was mixed with 50 mL of the grape-banana peel extract (GBPE). The mixture was boiled at a reaction time of 18 min at 60˚C with stirring maintained at 1000 rpm. The formation of a dark brown-coloured solution was an indication of the successful synthesis of the nanoparticles. Figure 1 clearly indicates the successful reduction of silver (Ag^{3+}) (Figure 1(b)) to Ag-NPs (Figure 1(c)) using GBPE (Figure 1(a)).

2.4. Electrochemical Analysis of GBPE capped Ag-NPs

Prior to analysis, glassy carbon electrodes were cleaned by polishing the electrodes on different alumina surfaces followed by thoroughly rinsing with distilled water. Thereafter, 4 µL of the synthesized nanoparticles was drop cast onto the electrodes and allowed to dry for 24 h. Analyses were initiated by placing the modified glassy electrode in a 3-electrode configuration cell together with Ag/AgCl reference and Pt wire counter electrode prior to analyses using cyclic voltammetry (CV) to study the electrochemical properties of the nanoparticles. The chosen potential window was from −1.5 V to 1.5 V and the analysis was achieved at different scan rates (10 - 100 mV/s).

2.5. Preparation for Studying Antibacterial Activities of Ag-NPs

The antibacterial activities of Ag-NPs were tested against *E. coli* 0157:H7 using

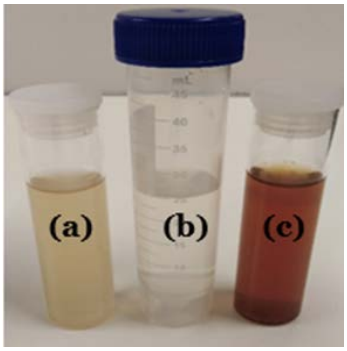

Figure 1. Photograph showing colour of solutions, (a) GBPE extract, (b) $AgNO_3$, (c) Ag-NPs.

the traditional disk diffusion method widely known as the Modified Kirby-Bauer susceptibility assay [25]. A single colony of glycerol stock *E. coli* 0157:H7 strain was grown overnight in a 20 mL Luria Broth (LB) medium. The media was then placed on a rotary shaker at 220 rpm at 37˚C to grow bacteria for 24 hours. Thereafter, the prepared bacterial suspension was serially diluted between 10 - 1016 CFU/mL with LB media in test tubes and a loop full of bacterial culture was placed on Thema Muller-Hinton agar (MHA) platets before placing 6 mm diameter disks impregnated with interventions on the plate (3 per plate). Three sets of plates were incubated with 10 µg/L concentration Ag-NPs in the following *E. coli* 0157:H7 volumes 100 µL, 150 µL and 200 µL, respectively and incubated at 37˚C for 24 hours. Thereafter, the average diameters of the zones of inhibition around the disks were determined by a Vennier calliper.

3. Results and Discussion

3.1. Optical Properties of GBPE-Ag-NPs

Studies have focused on the functionalization of silver nanoparticles using banana peel extract. However, there is currently no literature search that has thus far revealed the combination of grape and banana peel extracts (GBPE) for the synthesis of Ag-NPs. The attraction to these compounds is attributed to the fact that independently and in combination with silver metal precursors, banana peel and grapes have the ability to form biocompatible nanoparticles [26]. This study revealed increased stability and shelf life of the synthesized nanoparticles as opposed to the synthesis of the nanoparticles using the respective biological compounds. We hypothesize that it is the oxygen atoms from phenolic acid-type biomolecules found in both banana peels and grape-fruit that are responsible for the biosynthesis of Ag-NPs in this study [15]. Literature reports phenolic acid-type biomolecules to be responsible for the formation and stabilization of Ag-NPs [27]. This mechanism occurs according to Pearson's acid-base concept which elucidates that when a soft metal such as Ag+ specifically binds with a hard ligand, the chosen soft metal undergoes a reduction reaction since no complex compound is produced but instead the desired Ag-NPs are produced [16]. UV-Vis was used to follow the reduction of aqueous $AgNO_3$ ions during the reaction with GBPE. A strong absorption band at 440 nm was observed confirming the presence of Ag-NPs as shown in **Figure 2**, literature reports confirmed that silver nanoparticles absorb radiation in the visible regions of 400 - 500 nm [28]. Recently Masum and co-workers also confirmed the maximum wavelength (λ_{max}) of silver nanoparticles to be approximately 436 nm [29] while in another study by Kumar and co-workers it was obtained at 440 nm [30].

The visual observation of the reaction media changed, forming a dark brown colour, as shown previously in **Figure 1** illustrating the formation of Ag-NPs [31]. The colour of the reaction mixture started to change from pale brown to light brown within 9 min forming a dark brown solution after 12 min, as shown in **Figure 3**. As the reaction mixture became darker, more Ag-NPs were formed

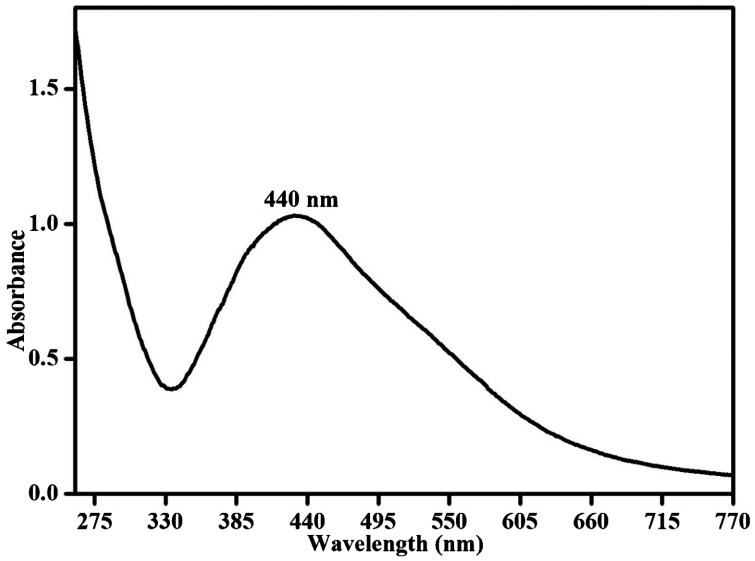

Figure 2. UV-Vis spectra of GBPE capped AgNPs.

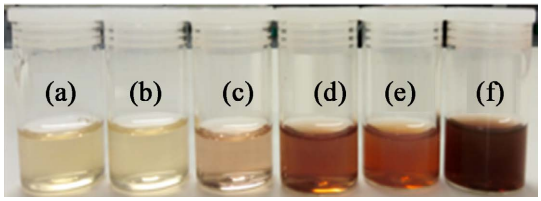

Figure 3. Visual inspection of the colour change of reaction solution in the process of Ag-NPs synthesis at different time intervals, (a) 3 min, (b) 6 min, (c) 9 min, (d) 12 min, (e) 15 min, (f) 18 min.

[32]. The brown colour arises due to the excitation of surface plasmon resonance (SPR) vibrations in the silver nanoparticles [33]. This is because silver nanoparticles have free electrons which give rise to SPR absorbance bands [34].

The intensity of SPR peaks was also seen to gradually increase during the synthesis of the nanoparticles with increased reaction time from 3 min until 18 min as shown in **Figure 4**. At 18 min, the maximum SPR peak was observed due to the depletion of silver ions (Ag^{+}) in the GBPE. The SPR band of silver nanoparticles shifts to the higher wavelength as the reaction time increases [35] [36] [37] indicating a redshift [38]. Redshift shows that there is a gradual increment in the mean diameter of GBPE-Ag-NPs [32]. The spectra show the reduction of Ag^{+} to Ago specifying the formation of Ag-NPs with a completed time of 18 min. The optimal time in this study was 18 min, which is relatively less than in other reports. For instance, Kumar and co-workers reported 60 min for Ag-NPs synthesised using *Hydnocarpus pentandra* leaves [39].

3.2. FT-IR Analysis of BGPE-AgNPs

FT-IR was employed to validate the major functional groups in the extract and their involvement in the synthesis and stabilization of the synthesized silver nanoparticles. **Figure 5** represents the spectra of GBPE (black curve) and the

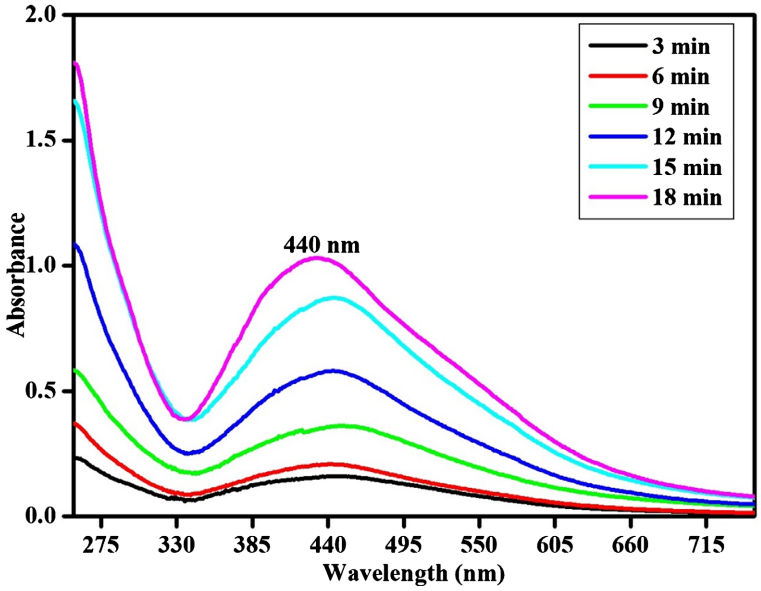

Figure 4. UV-Vis spectra of GBPE capped Ag-NPs at different time intervals.

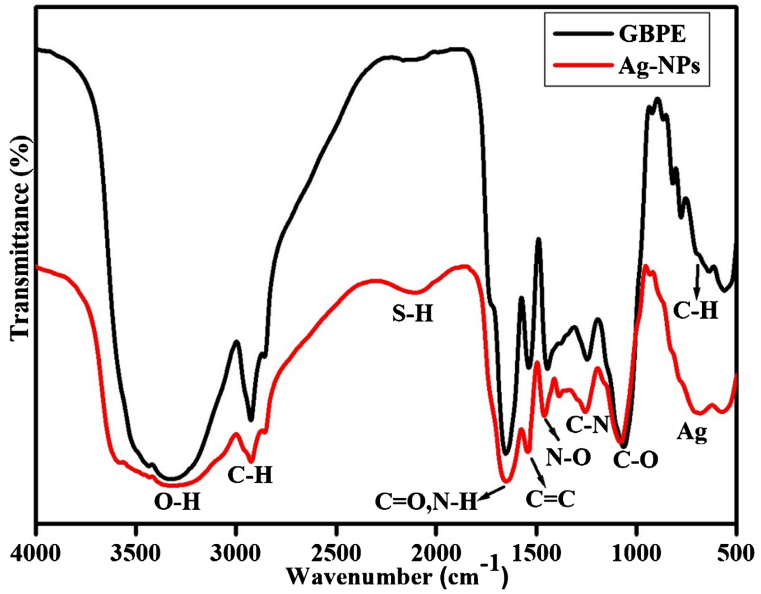

Figure 5. FT-IR spectra of the green synthesised Ag-NPs and GBPE.

synthesized Ag-NPs (red curve) where they were compared in order to investigate the changes before and after the reaction with peak assignment. Similar spectra between the extract and colloidal solution were obtained as shown in indicating that the same compounds existed before and after the reaction. Although the similarities were observed, some of the absorption peaks are seen to be shifted in their position after the addition of $AgNO_3$.

From the FT-IR spectra, the presence of the sharp O-H peak at 3366 cm^{-1} was due to the stretching vibrations of hydroxyl groups (-OH) of alcohol and phenols [40]. The sharp peak at 2922 cm^{-1} in GBPE represents the O–H stretching vibration bands characteristic of carboxylic acids and C-H stretches from al-

kanes. Hence, the synthesised Ag-NPs are stabilized and coated by functional groups that are present in the GBPE [41]. The functional groups that are present within GBPE include polysaccharides such as cellulose as well as the phytochemical carotenoid [42] [43]. The reduced peak intensities in the spectrum indicate that the affected groups are involved in the formation of the nanoparticles.

The FT-IR spectrum of Ag-NPs showed a band at 3270 cm^{-1} for hydrogen-bonded stretching vibrations attributed by phenol and alcohol groups. The weak peak at 2093 cm^{-1} is due to thiols S-H stretching vibrations indicating the presence of the banana peel in the GBPE extract. The peak observed at 1725 cm^{-1} was assigned as the stretching vibration of C=O from carboxylic acids (found in bananas), ketones (found in grapes) and aldehydes (found in grapes). The peak at 1633 cm^{-1} is characteristic of C=C stretching vibrations attributed to alkene groups (found in grapes). The bands at 1407 and 1253 cm^{-1} are due to the presence of aromatic rings and nitro compounds while the C=C, N-O and C-N stretching vibrations are due to amine groups, the intense peaks at 1407 and 1253 cm^{-1} were assigned due to nitriles in the GBPE [44]. These peaks were reduced in intensity as compared to the Ag-NPs spectrum revealing the involvement of nitrile groups from the extracts as the capping agents for the nanoparticles. The weak peak at 636 cm^{-1} corresponds to asymmetric stretching vibrations of C-H groups in the GBPE as shown in the spectrum and seen to disappear in the spectrum of Ag-NPs due to its participation in the synthesis process. The Ag-NPs spectrum also indicates another peak at 585 cm^{-1} caused by the stretching vibrations of the nanoparticles thus confirming the formation of nanoparticles [45]. Finally, that amine, hydroxyl and carboxyl groups were responsible for the formation of the novel silver nanoparticles while the phenolic compounds that were present in the extract were the driving force in the formation of the nanoparticles. The obtained results are similar to a recent report by Singh and co-workers who reported the synthesis of Ag-NPs using *Rhodiola Rosea rhizome* extract [46]. Hence from the above analysis, we concluded that amine, hydroxyl and carboxyl groups present in the extract played a significant role in the reduction of Ag^{+} ion into Ag-NPs.

3.3. Particle Size and Shape Analysis of BGPE-AgNPs

HRTEM was used to determine the size and the shape of the bio-synthesized Ag-NPs. **Figure 6(a)** shows the HRTEM image with a scale view of 200 nm shows the GBPE capped Ag-NPs to be predominantly poly-dispersed and spherical in shape with sizes ranging from 25 to 39 nm, which agrees with the shape of the SPR band in the UV-vis spectrum [47]. Similar results of spherical Ag-NPs shape were obtained using different fruit extracts such as *Phoenix dactylifera* extract and Watermelon rind extract [48]. Furthermore, the lattice fringes visible in **Figure 6(b)** indicates good crystallinity and the lattice spacing (d-spacing) was determined to be 0.231 nm. This spacing is known as inter-planar spacing (d-spacing) which is in between the vertical lattice fringes, indicating the space between the XRD Braggs reflection. According to Liang and co-workers, an

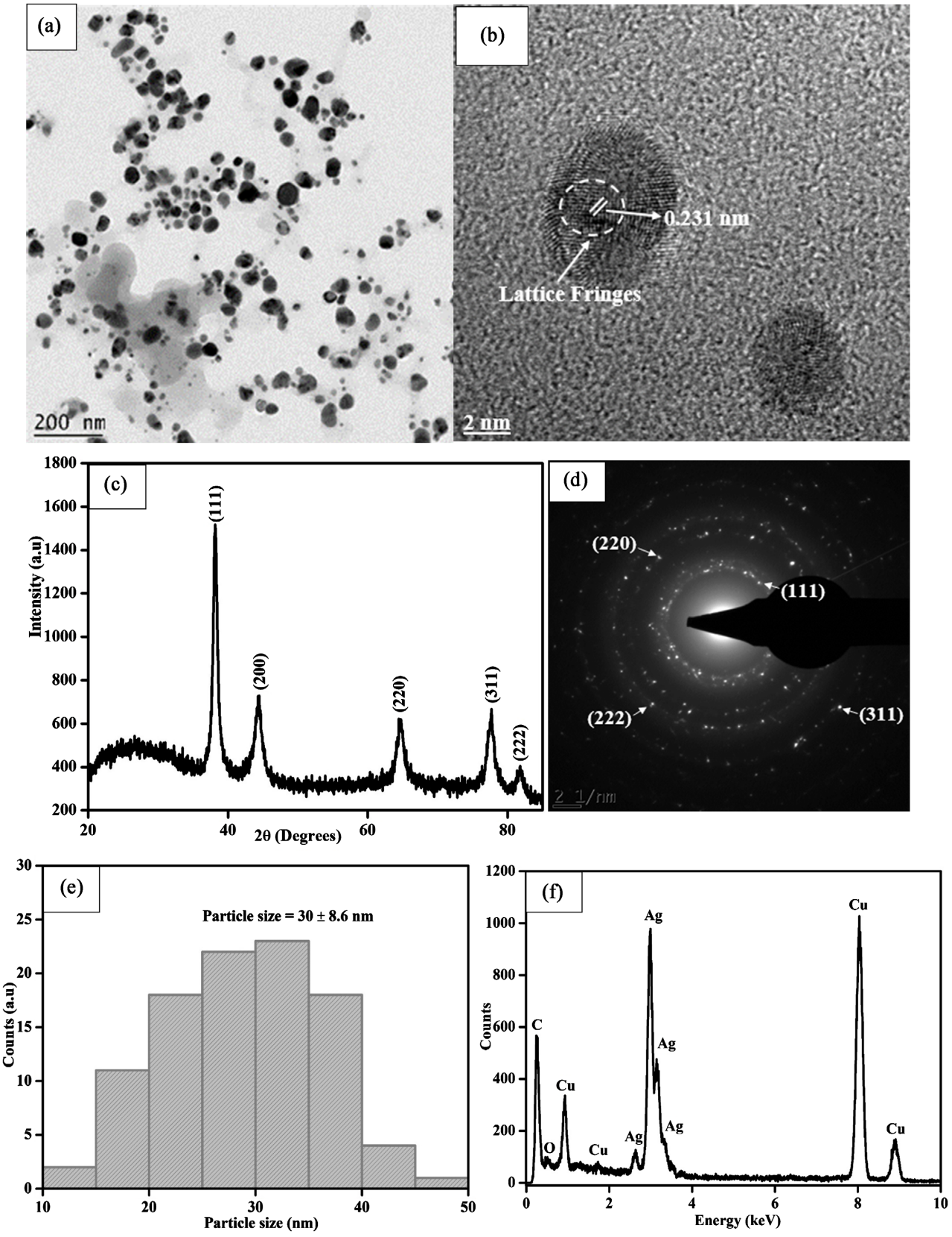

Figure 6. (a) HR-TEM image of Ag-NPs at 200 nm range, (b) lattice fringes, (c) X-ray diffraction pattern, (d) Selected area electron diffraction (SAED) patterns, (e) histogram, (f) Energy Dispersive Spectroscopy patterns of GBPE capped Ag-NPs.

interlayer spacing of 0.231 nm corresponds to the lattice spacing of the silver (111) planes [49] [50]. Gomati and co-workers also reported lattice spacing of 0.23 nm for Ag-NPs synthesised using *Datura stramonium* leaves [51].

Figure 6(c) confirms the crystalline nature of the nanoparticles and the five intense diffraction patterns obtained in the spectrum of nanoparticles correspond to the standard metallic silver JCPDF NO:04-0873 [52]. Aruna and Jarayaman reported similar results for green synthesised silver nanoparticles using *Gum tragac*anth [53] while Dong and co-workers also reported similar results using wolfberry fruit [47]. **Figure 6(d)** shows the selected area electron diffraction (SAED) illustrating the following five Braggs reflection rings (111), (200), (220), (311), and (222) planes an indication that the nanoparticles are highly crystalline [54]. The SAED pattern is in good agreement with XRD (**Figure 6(c)**) findings where intense Bragg reflection peaks at 38.17, 44.43, 64.58 and 77.64 corresponding to the silver crystal planes (111), (200), (220), (311) and (222) an indication of face centered cubic crystalline structured metallic silver [55]. The average particle size of the nanoparticles was determined to be 30 nm based on the full-width half maximum (FWHM) data using Scherer's equation (Equation 1.1,). Similar reflections were also observed in the XRD spectrum of the green synthesised silver nanoparticles using *Vitex Negudo* [56], sufron waste [57], and *Azadirachta indica* leaf [58]. The particle size distribution histogram of the synthesized Ag-NPs shown in **Figure 6(e)** corresponded well with values obtained from HRTEM and XRD measurements.

The energy-dispersive x-ray spectroscopy (EDS) of the nanoparticles illustrated in **Figure 6(f)** shows the presence of the silver elements at 3 KeV, which confirms the formation of silver nanoparticles [59]. The presence of carbon and oxygen in the sample was also found due to the presence of polyphenol groups originating from the extract and are bound to the surface of silver nanoparticles thus indicating the reduction of silver ions (Ag^{+}) to elemental silver (Ag). The analysis further shows the presence of copper contributed by the copper grid on to which the sample was coated. No other peaks were observed in the spectrum, confirming the complete reduction of silver compounds to silver nanoparticles [60]. Previously obtained reports similar to these results were also reported by [61] [62].

$$d = \frac{K\lambda}{\beta \cos \beta} \tag{1.1}$$

where: d = particle/crystal size, K is a constant and can be defined as the dimensionless shape factor and is equal to 0.94 K usually range from 0.5 - 1, and λ is the X-ray wavelength (0.154 nm), β is the full-width half-maximum (FWHM in radians), θ is the angle of reflection [63].

3.4. Internal Structure Analysis of BGPE-AgNPs

Small Angle X-Ray Spectroscopy (SAXS) was employed to determine the precise size distribution, shape, and internal structure of the synthesized Ag-NPs. As can

be seen in **Figure 7(a),** the SAXS free model pair-distance distribution function (PDDF) of the GBPE capped Ag-NPs revealed a spherically characteristic profile typically observed for poly-dispersed nanoparticles with the largest particle size detected to have a diameter of 39 nm [26]. Agglomerated particles also appeared at 35 nm which is illustrated by a hump. [64] [65]. **Figure 7(b)** reveals the size distribution weighted by number (black line) and intensity (red line) where the Ag-NPs highly revealed poly-dispersed particles with average radii of (13 nm, 20 nm and 29 nm), respectively [27]. Most of the particles appeared at 4 nm for weighted by number and 29 nm for intensity distribution functions. The size of 29 nm is close to the determined values as reported by HR-TEM. However, the appearance of an enhanced peak at 29 nm was also ascribed to distribution by intensity. Since, the colloidal suspensions consist of poly-dispersed particles and the measured scattering intensity represents the sum of the scattering intensities from particles of various sizes [28]. This is given by Equation (1.2):

$$I(q) = NV(p - p_0)^2 \int_0^{\infty} \left(\frac{\pi d^3}{6}\right)^2 f(d) P(q,d) \mathrm{d}d \tag{1.2}$$

where $f(d)$ is the particle size distribution by number.

3.5. CV Analysis of GBPE Capped Ag-NPs

In this study, the electrochemical analyses of Ag-NPs were performed in order to monitor the characteristic features of the novel GBPE-AgNPs. **Figure 8(a)** shows the CV voltammograms of the bare GCE as well as the GBPE-Ag-NPs/GCE modified electrode in 0.2 M PBS, pH 7.4 electrolyte solution. As can be seen, the GBPE-Ag-NPs exhibited one pair of redox peaks (E_{pc} = 0.75 V and E_{pa} = 0.16 V), which are attributed to the oxidation and reduction of Ag ions. Similar observations were reported by Blake and core-workers [66]. On the other hand, Lima and co-workers also observed an oxidation peak in the same region which (0.24 V) which was associated with the conversion of Ag^{+}/Ag^{o} and also indicated the

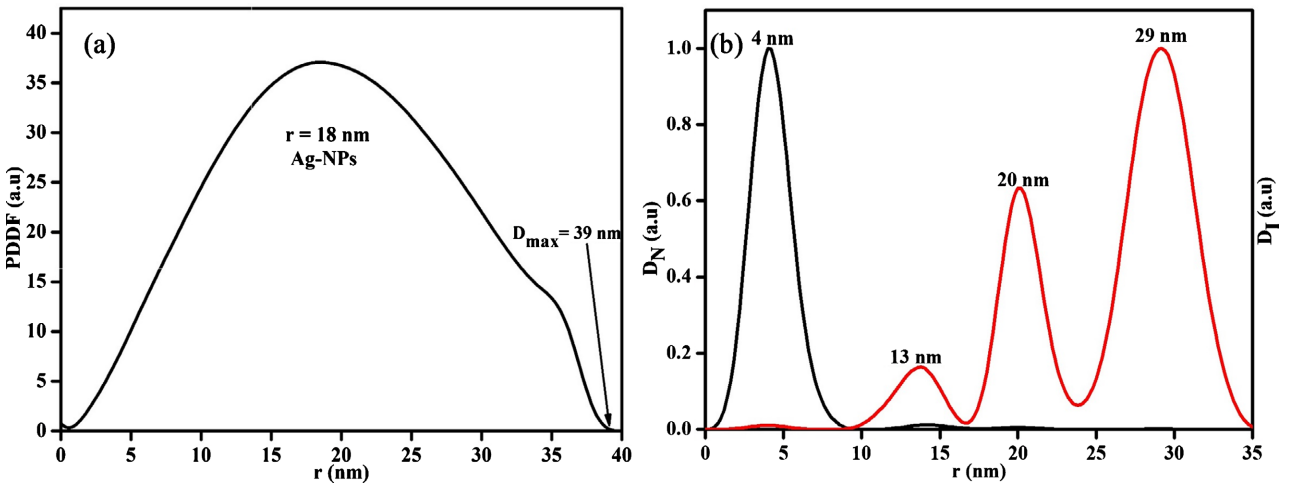

Figure 7. (a) SAXS pair distance distribution function (PDDF) of GBPE AgNPs. (b) Size distribution functions weighted by number (black line) and intensity (red line).

presence of Ag-NPs [67]. The voltammograms illustrated in **Figure 8(b)** reveal increased currents with increasing scan rates (10 - 100 mV/s) during the electrochemical analysis of Ag-NPs. The redox peak currents increased with increasing scan rates while a shift in the potential was observed to more positive values [29]. This is indicative of electro-active nanoparticles with potential applications in sensor development Additionally, the diffusion coefficient denoted as (D_e) of the GBPE-Ag-NPs/GCE electrode was determined to be 5.22×10^{-5} cm^2 s^{-1} using the Randel-Sevcik equation (Equation (1.3)) while the surface concentration was determined to be 2.31×10^{-5} mol cm^{-2} using the Brown-Anson method (Equation 1.4). The obtained D_e was larger compared to the previously reported in literature and therefore larger values of D_e indicates a faster motion of analyte through the solution whereas small values of D_e indicates slower motion. Khan and co-workers reported a D_e value of 7.6×10^{-6} $cm^2 \cdot s^{-1}$ using Ag-NP-MWCNT-GCE which was lower compared to this study [68].

$$I_p = 0.4463nFAC\left(\frac{nFvD_{eAu-NPs}}{RT}\right)^{1/2} \tag{1.3}$$

$$I_p = \frac{n^2F^2\Gamma^*_{Au-NPs}Av}{4RT} \tag{1.4}$$

3.6. Bacterial Detection

Surface Plasmon Resonance Detection

In this study we investigated the potential detection effects of Ag-NPs synthesized using a mixture of banana peel and grapes. To confirm the effect of the nanoparticles, a comparative study of the Ag-NPs before and after the interaction with *E. coli* 0157:H7 was performed using UV-vis spectrophotometer. **Figure 9(a)**, shows the UV-Vis spectra of silver nanoparticles before and after their interaction with *E. coli* 0157:H7 at different concentrations. As seen from **Figure 9(a)**, silver nanoparticles in the absence of *E. coli* 0157:H7 show an SPR

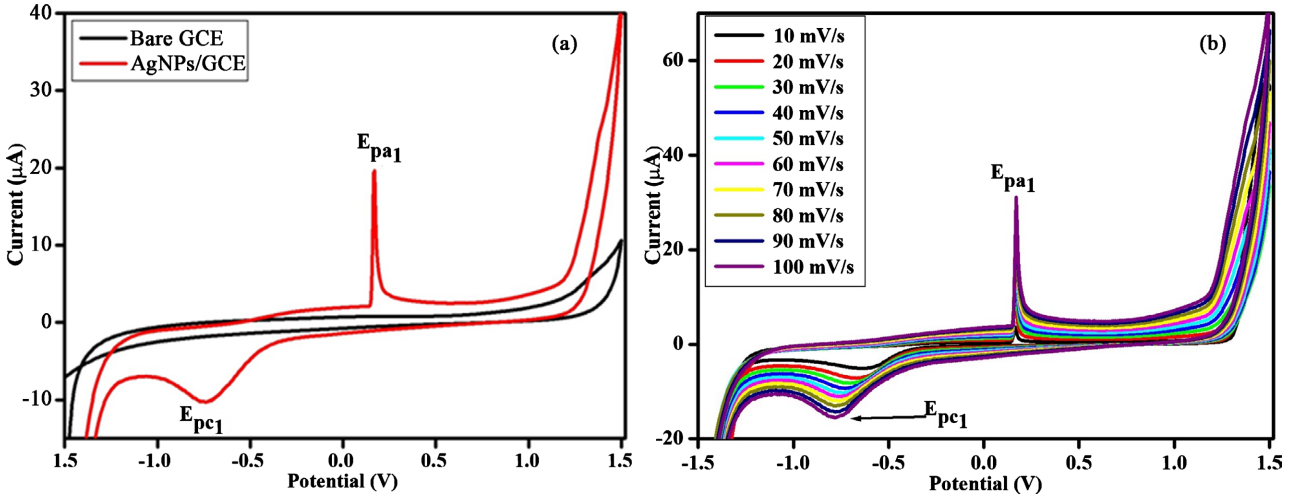

Figure 8. (a) Cyclic voltammogram of bare GCE (Black line), Ag-NPs|GCE (Red line) recorded in 0.2 PBS, pH 7.4 at 50 mV/s, (b) Multi-Scan Voltammograms of Ag-NPs in 0.2 PBS, pH 7.4 at (10 - 100 mV/s).

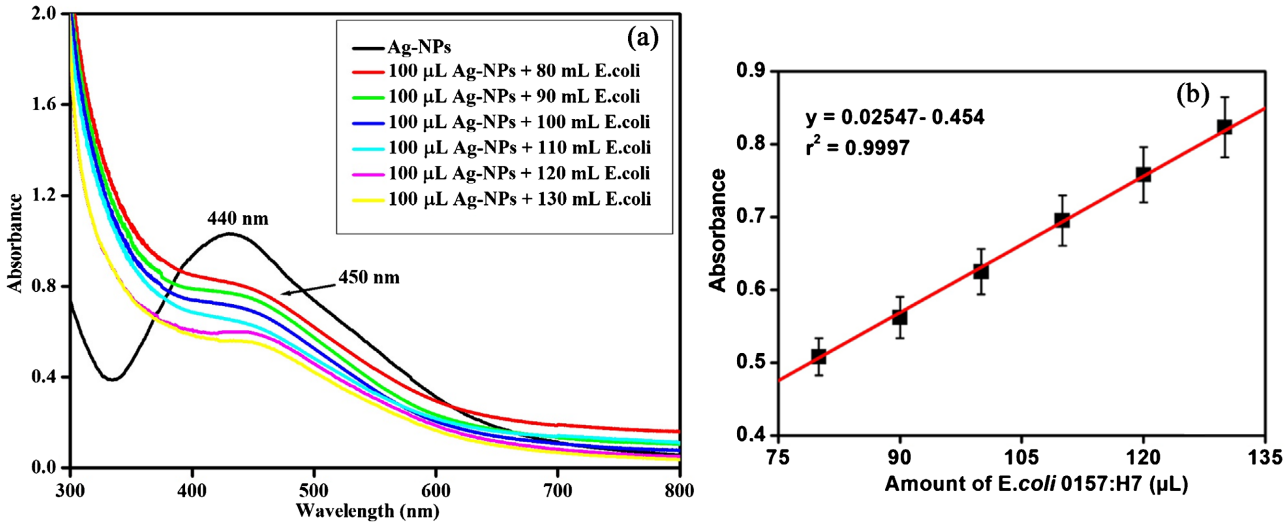

Figure 9. (a) Detection of *E. coli* 0157:H7 in seawater, Ag-NPs before the interaction (Black line) with the interaction of *E. coli* at different concentration (other). (b)Calibration curve for surface plasmon resonance response corresponding to different values and the volume of *E. coli* 0157:H7 bacteria in a range of 80 - 130 µL.

band at 440 nm in water (black spectrum). In the presence of *E. coli* 0157:H7 in water, we observed a reduction in the peak intensity with a redshift taking place at the same time. The decrease in peak intensity is the evidence of the interaction between Ag-NPs and bacteria. The redshift was observed by the change in SPR to more extended wavelength regions from 440 nm to 450 nm [69] which is due to many factors such as capping agent replacement, surface plasmon coupling or aggregation or agglomeration between closely spaced nanoparticles [70]. Similar results were reported by Boken and co-workers who also observed changes in SPR bands from 395 nm before the interaction to 408 nm after the interaction with *E. coli* 0157:H7 when using robust silver nanoparticle [71]. **Figure 9(b)** show a calibration plot with a good linear relationship plotted using the SPR response versus the different volumes of *E. coli* 0157:H7 from 80 - 130 µL. The plot shows a linear equation of (y = 0.02547 - 0.454) with a correlation coefficient of (0.9997). Similar results were reported by Wang and co-workers who observe a linear relationship with correlation coefficient of (0.9938).

In this research study, the limit of detection was determined using (Equation 1.5). The limit of detection (LOD) is the lowest concentration that can be measured or detected, and it was found to be 1×10^2 CFU/mL [72] [73]. A study by Yaghubi and co-workers reported similar results using Au-NPs conjugated with antibodies [74]. Our results were much lower or better compared to the reported literature, for example, Haicao and co-workers reported LOD of 2×10^8 CFU/mL using mercaptoethylamine modified Au-NPs for *E. coli* O157:H7 [75]. **Table 1** shows detection limits obtained in studies where *E. coli* 0157:H7 bacteria were detected using Surface Plasmon Resonance (SPR) sensors. From the table, it is evident that this study illustrated data far better in comparison to the previously reported studies from the literature. Therefore, the developed sensor can detect *E. coli* 0157:H7 in water using green synthesised nanoparticles without

Table 1. Comparison of LOD on SPR sensor for detection *E. coli* 0157:H7 using different material.

Material Used	Technique Used	LOD CFU/mL	Reference
3-MPA-Au-NPs	SPR	1.8×10^3	[78]
Magnetic Ag-NPs	SPR	4.8×10^5	[79]
Magnetic NPs	SPR	1.0×10^5	[80]
AgNPs-rGO bimetallic	SPR	5.0×10^2	[81]
GBPE-Ag-NPs	SPR	1.0×10^2	This Work

the support of antibodies. The developed sensors can achieve detection within 3 min, during which the bacterium has sufficient time to bind and for analysis to be achieved. The obtained detection limit in this study falls within the range 1×10^{-3} to 1×10^7 CFU/mL of the currently accepted methods reported in the literature [76] [77].

$$LOD = 3.3\frac{S}{M} \tag{1.5}$$

From the equation, 3.3 is the coefficient, S represents the value of the standard deviation of the blank samples, and M is the slope of the standard curve within the concentration range.

3.7. Electrochemical Detection

Various *E. coli* concentrations from 1×10^1 to 1×10^6 CFU/mL were prepared through serial dilution method as described in the previous studies. The electrochemical detection of *E. coli* was performed immediately after 24 h incubation period. The electrochemically active GBPE-Ag-NPs were electrodeposited on GCE. The choice of this electrode was made due to the cost-effective nature of the electrode as well as its reliable and stable properties. Panhawar and co-workers studied three different electrodes namely (glassy carbon electrode, platinum electrode and screen-printed electrode) for the detection of *E. coli*, and they reported GCE as the better electrode for the detection of *E. coli* [82]. All the experiments were performed at optimum conditions at the potential window of −1.5 to 1.5 V, using a scan rate of 50 mV/s under continuous magnetic stirring as, and a sample of 100 µL was analyses from each bacterial concentration. The green synthesised nanoparticles analyses were used to detect targeted bacteria by measuring the electrochemical response of the nanoparticles before and after their interaction with the bacteria. The functionalised nanoparticles show enhanced current responses before their interaction with *E. coli*. **Figure 10(a)** shows GBPE-Ag-NPs|GCE detecting different concentrations of *E. coli* 0157:H7 in PBS solution (0.2 M pH 7.4) and the (black) represents GBPE-Ag-NPs|GCE before interaction with *E. coli* 0157:H7. Following the interaction, the movement of electrons on GCE is reduced due to the presence of other materials, indicating that the bacteria detection has occurred. Shin and co-workers reported similar

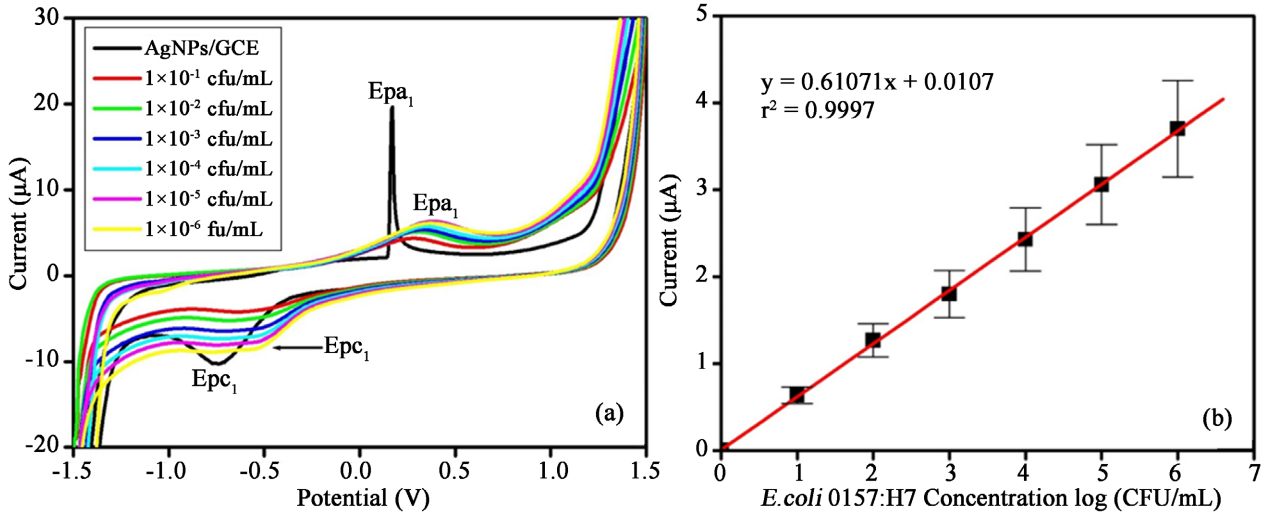

Figure 10. (a) GBPE Ag-NPs/GCE modified electrode with different concentration of *E. coli* 0157:H7 in PBS solution (0.2 M pH 7.4). (b) Calibration curve for electrochemical response corresponding to different concentration of *E. coli* 0157:H7 bacteria in a range of 10^1 to 10^6 CFU/mL.

behaviour, in the detection of *E. coli* in river water using Prussian blue coated with titanium dioxide particles [83]. From the plots, a change of electrochemical signal was observed due to the interaction of nanoparticles with *E. coli*. The change in current response or electrochemical signal, anodic (I_{pa}) and cathodic (I_{pc}) peak current response before the interaction of GBPE-Ag-NPs|GCE with *E. coli* is compared with the current response after the interaction with *E. coli* 0157:H7. The change in the current response for the anodic peak (I_{pa1}) = 18.777 μA and cathodic peak currents (I_{pc1}) = 0.738 μA peaks before the interaction of GBPE-Ag-NPs|GCE with *E. coli* 0157:H7 compared with the current response after the interaction with anodic (I_{pa1}) = 6.851 μA and cathodic (I_{pc1}) = −8.235 μA indicate the presence of *E. coli*. Similar results were reported by Klabunde and co-workers when using highly reactive metal oxide nanoparticles to treat *E. coli* *[84]*. As the concentration of *E. coli* increases the current response also increases due to the interaction between *E. coli* and nanoparticles. Thus, the concentration of the *E. coli* has a linear relationship with the current. **Figure 10(b)** is the calibration curve (N = 3) of the GBPE-Ag-NPs|GCE with a good linear relationship between the current response and the logarithms of different concentrations of *E. coli* 0157:H7. The linearity that was accomplished from the graph was used to calculate linear regression equation which was (r^2 = 0.9997) and the slope was used to calculate the LOD. The slope of the calibration also gives information about the sensitivity of the sensor, the higher the slope of the calibration curve the higher the sensitivity of the sensor for that specific component [85]. Therefore, the slope was determined to be 0.61071 μA/CFU/mL. The sensitivity of GBPE|Ag-NPs|GCE was more improved compared to the reported sensors in literature, for example our sensitivity was higher than the recently reported study by Cimafonte and co-workers using a Impedimetric Immunosensor based on a screen printed electrode for detection of *E. coli* [86]. The sensing potential

Table 2. Limit of Detection of more relevant studies reported in the literature for detection of *E. coli* 0157:H7 compared to this study.

Material used	Electrode used	LOD (CFU/mL)	Reference
Au-NPs modified with antibodies	Screen-printed carbon electrodes (SPCEs)	3.09×10^2	[87]
CDs/ZnO nanorod/PANI	SPCE	8.00×10^7	[88]
Pt-NPs	GCE	20	[89]
Multi-walled carbon nanotubes	GCE	6.2×10^5	[90]
GBPE Ag-NPs	GCE	3.5×10^1	This work

of GBPE-Ag-NPs|GCE for our experimental results showed LOD of 3.5×10^1 CFU/ mL **Table 2** shows the limit of detection of more relevant electrochemical studies reported in the literature for the detection of *E. coli* 0157:H7 compared to this study. From the table, it is evident that the results obtained in this study were better compared to previous reports. Therefore, the developed sensor can detect *E. coli* 0157:H7 in water using green synthesised nanoparticles without any further modifications. The electrochemical detection process takes 45 min, which is less than 1 hr for the bacterium to bind and for analysis to commence. Therefore, our research findings show a better approach for the detection of *E. coli* 0157:H7.

4. Conclusion

A green and novel synthesis method for the synthesis of silver nanoparticle biosynthesized with a mixture of banana peel and grape extracts was achieved for the first time. The proposed procedure is simple and easy to scale up, not to mention the green aspect eliminating the need for any additional chemicals. FT-IR was used to identify the type of functional groups that were responsible for the reduction of Ag^+ ions and to also identify the type of functional groups that are coated or capped on Ag-NPs. The poly-dispersed and spherical nature of the nanoparticle was confirmed by XRD, HR-TEM and SAX. Finally, glassy carbon Ag-NPs modified electrodes revealed that electroactive nanomaterials with high electron transport an indication that these nanoparticles have potential application in sensor development. Additionally, the benefit of this method lays in the stability and prolonged shelf-life of the synthesized nanoparticles a great need in various other applications of Ag-NPs. Furthermore, the biosynthesized Ag-NPs nanoparticles displayed solid level of antibacterial activity against *E. coli* indicating that they could be used as effective pathogen agents for potentially useful biomedical applications.

Acknowledgements

The authors are grateful for funding from the National Research Foundation, South Africa for funding this research study. Our gratitude also goes to the

Council for Scientific and Industrial Research, South Africa for providing bursaries to the students involved in this study.

Conflicts of Interest

The authors declare no conflicts of interest regarding the publication of this paper.

References

[1] Mailu, S.N., Waryo, T.T., Ndangili, P.M., Ngece, F.R., Baleg, A.A., Baker, P.G. and Iwuoha, E.I. (2010) Determination of Anthracene on Ag-Au Alloy Nanoparticles/Overoxidized-Polypyrrole Composite Modified Glassy Carbon Electrodes. *Sensors* (*Switzerland*), **10**, 9449-9465. https://doi.org/10.3390/s101009449

[2] Ajiboye, T.O., Babalola, S.O., Fadiji, A.E. and Onwudiwe, D.C. (2022) Green Synthesis of Zinc Oxide Nanoparticles Using Plantain Peel Extracts and the Evaluation of Their Antibacterial Activity. *Scientific African*, **16**, e01152. https://doi.org/10.1016/j.sciaf.2022.e01152

[3] Baum, R. and Bartram, J. (2018) A Systematic Literature Review of the Enabling Environment Elements to Improve Implementation of Water Safety Plans in High-Income Countries. *Journal of Water and Health*, **16**, 14-24. https://doi.org/10.2166/wh.2017.175

[4] Huang C. K., Mukhopadhyay, R., Wen, B., Gitai, Z. and Wingreen, N.S. (2008) Cell Shape and Cell-Wall Organization in Gram-Negative Bacteria. *Proceedings of the National Academy of Science of the United States of America*, **105**, 19282-19287. https://doi.org/10.1073/pnas.0805309105

[5] Chibuike, A.N., John, A., Umar, U., John, E., Amechi, O.I., Emmanuel, U.A. and Emmanuel, N.N. (2020) Bacteriophages as Bio-Control Agent against Food-Borne Pathogen *E. coli* O157:H7. *International Journal of Pharmacy and Biological Sciences*, **15**, 23-36.

[6] Yin, H., Gupta, N., Chen, C., Boomer, A., Pradhan, A. and Patel, J. (2020) Persistence of *Escherichia coli* O157:H12 and *Escherichia coli* K12 as Non-Pathogenic Surrogates for O157:H7 on Lettuce Cultivars Irrigated with Secondary-Treated Wastewater and Roof-Collected Rain Water in the Field. *Frontiers in Sustainable Food Systems*, **4**, Article 555459. https://doi.org/10.3389/fsufs.2020.555459

[7] Akindolire, M.A. and Ateba, C.N. (2019) Complete Genome Sequence of *Escherichia coli* O157:H7 Phage PhiG17. *Microbiology Resource Announcements*, **8**, e01296. https://doi.org/10.1128/MRA.01296-18

[8] Mhlongo, S., Mativenga, P.T. and Marnewick, A. (2018) Water Quality in a Mining and Water-Stressed Region. *Journal of Cleaner Production*, **171**, 446-456. https://doi.org/10.1016/j.jclepro.2017.10.030

[9] Kaushik, M., Nandi, A.V. and Mungurwadi, V.B. (2018) Portable Sensors for Water Pathogens Detection. *Materials Today Proceedings*, **5**, 10821-10826. https://doi.org/10.1016/j.matpr.2017.12.368

[10] Luyt, C.D., Tandlich, R., Muller, W.J. and Wilhelmi, B.S. (2012) Microbial Monitoring of Surface Water in South Africa: An Overview. *International Journal of Environmental Research and Public Health*, **9**, 2669-2693. https://doi.org/10.3390/ijerph9082669

[11] Dufour, A.P., Strickland, E.R. and Cabelli, V.J. (1981) Membrane Filter Method for

Enumerating *Escherichia coli*. *Applied and Environmental Microbiology*, **41**, 1152-1158. https://doi.org/10.1128/aem.41.5.1152-1158.1981

[12] Edberg, S.C., Allen, M.J., Smith, D.B., LeChevallier, M., Kriz, N., Callan, D., Ward, R., Calvert, D., Hmurciak, L., Trok, T., Burns, M., Shinn, V., Kraus, B., Dery, C., Coluccio, V. and Iwan, J. (1989) National Field Evaluation of a Defined Substrate Method for the Simultaneous Detection of Total Coliforms and *Escherichia coli* from Drinking Water: Comparison with Presence-Absence Techniques. *Applied and Environmental Microbiology*, **55**, 1003-1008. https://doi.org/10.1128/aem.55.4.1003-1008.1989

[13] Leoni, E., De Luca, G., Legnani, P.P., Sacchetti, R., Stampi, S. and Zanetti, F. (2005) Legionella Waterline Colonization: Detection of Legionella Species in Domestic, Hotel and Hospital Hot Water Systems. *Journal of Applied Microbiology*, **98**, 373-379. https://doi.org/10.1111/j.1365-2672.2004.02458.x

[14] Brooks, B.W., Devenish, J., Milnes, D. and Robertson, R.H. (2004) Evaluation of a Monoclonal Antibody-Based Enzyme-Linked Immunosorbent Assay for Detection of *Campylobacter fetus* in Bovine Preputial Washing and Vaginal Mucus Samples. *Veterinary Microbiology*, **103**, 77-84. https://doi.org/10.1016/j.vetmic.2004.07.008

[15] Bej, A.K., Mahbubani, M.H., Dicesare, J.L. and Atlas, R.M. (1991) Polymerase Chain Reaction-Gene Probe Detection of Microorganisms by Using Filter-Concentrated Samples. *Applied and Environmental Microbiology*, **57**, 3529-3534. https://doi.org/10.1128/aem.57.12.3529-3534.1991

[16] Ruan, C., Yang, F., Lei, C. and Deng, J. (1998) Thionine Covalently Tethered to Multilayer Horseradish Peroxidase in a Self-Assembled Monolayer as an Electron-Transfer Mediator. *Analytical Chemistry*, **70**, 1721-1725. https://doi.org/10.1021/ac970605m

[17] Behrendorff, J.B.Y.H. and Gillam, E.M.J. (2016) Prospects for Applying Synthetic Biology to Toxicology: Future Opportunities and Current Limitations for the Repurposing of Cytochrome P450 Systems. *Chemical Research in Toxicology*, **30**, 453-468. https://doi.org/10.1021/acs.chemrestox.6b00396

[18] Nasrollahzadeh, M. and Mohammad Sajadi, S. (2016) Green Synthesis, Characterization and Catalytic Activity of the Pd/TiO_2 Nanoparticles for the Ligand-Free Suzuki-Miyaura Coupling Reaction. *Journal of Colloid and Interface Science*, **465**, 121-127. https://doi.org/10.1016/j.jcis.2015.11.038

[19] Duan, S. and Wang, R. (2013) Bimetallic Nanostructures with Magnetic and Noble Metals and Their Physicochemical Applications. *Progress in Natural Science*: *Materials International*, **23**, 113-126. https://doi.org/10.1016/j.pnsc.2013.02.001

[20] Bahrulolum, H., Nooraei, S., Javanshir, N., Tarrahimofrad, H. and Mirbagheri, V.S. (2021) Green Synthesis of Metal Nanoparticles Using Microorganisms and Their Application in the Agrifood Sector. *Journal of Nanobiotechnology*, **19**, 1-26. https://doi.org/10.1186/s12951-021-00834-3

[21] Kumar, H., Bhardwaj, K., Dhanjal, D.S. and Nepovimova, E. (2020) Fruit Extract Mediated Green Synthesis of Metallic Nanoparticles: A New Avenue in Pomology Applications. *International Journal of Molecular Sciences*, **21**, Article No. 8458. https://doi.org/10.3390/ijms21228458

[22] Journal, A.I., Rafique, M., Sadaf, I., Rafique, M.S. and Tahir, M.B. (2017) A Review on Green Synthesis of Silver Nanoparticles and Their Applications. *Artificial Cells, Nanomedicine, and Biotechnology*, **45**, 1272-1291. https://doi.org/10.1080/21691401.2016.1241792

[23] Kuppusamy, P., Yusoff, M.M. and Govindan, N. (2014) Biosynthesis of Metallic

Nanoparticles Using Plant Derivatives and Their New Avenues in Pharmacological Applications—An Updated Report. *Saudi Pharmaceutical Journal*, **24**, 473-484. https://doi.org/10.1016/j.jsps.2014.11.013

[24] Bastos-arrieta, J., Florido, A., Clara, P. and Serrano, N. (2018) Green Synthesis of Ag Nanoparticles Using Grape Stalk Waste Extract for the Modification of Screen-Printed Electrodes. *Nanomaterials* (*Basel*), **8**, Article No. 946. https://doi.org/10.3390/nano8110946

[25] Campbell, B. (2012) Technical Section. *Annals of the Royal College of Surgeons of England*, **94**, 359. https://doi.org/10.1308/rcsann.2012.94.5.359

[26] Zhou, G.J., Li, S.H., Zhang, Y.C. and Fu. Y.F. (2014) Biosynthesis of CdS Nanoparticles in Banana Peel Extract. *Journal of Nanoscience and Nanotechnology*, **14**, 4437-4442. https://doi.org/10.1166/jnn.2014.8259

[27] Iravani, S., Korbekandi, H., Mirmohammadi, S.V. and Zolfaghari, B. (2014) Synthesis of Silver Nanoparticles: Chemical, Physical and Biological Methods. *Research in Pharmaceutical Science*, **9**, 385-406.

[28] Mawaddah, M.O., Pambudi, A.B., Pratiwi, A.R. and Kurniawan, F. (2018) Green Synthesis of Silver Nanoparticles Using Photo-Induced Reduction Method. *AIP Conference Proceedings*, **2049**, Article ID: 020082. https://doi.org/10.1063/1.5082487

[29] Masum, M.M.I., Siddiqa, M.M., Ali, K.A., Zhang, Y., Abdallah, Y., Ibrahim, E., Qiu, W., Yan, C. and Li, B. (2019) Biogenic Synthesis of Silver Nanoparticles Using *Phyllanthus emblica* Fruit Extract and Its Inhibitory Action Against the Pathogen *Acidovorax oryzae* Strain RS-2 of Rice Bacterial Brown Stripe. *Frontiers in Microbiology*, **10**, Article No. 820. https://doi.org/10.3389/fmicb.2019.00820

[30] Kumar, B., Smita, K., Cumbal, L. and Debut, A. (2016) *Ficus carica* (Fig) Fruit Mediated Green Synthesis of Silver Nanoparticles and Its Antioxidant Activity: A Comparison of Thermal and Ultrasonication Approach. *Bionanoscience*, **6**, 15-21. https://doi.org/10.1007/s12668-016-0193-1

[31] Garibo, D.D., Nuñez, H.A.B., De León, J.N.D., Mendoza, E.G., Estrada, I., Magaña, Y.T., Tiznado, H., Marroquin, M., Ramos, A.G.S., Blanco, A., Rodríguez, J.A., Romo, O.A., Almazán, L.A.C. and Arce, A.S. (2020) Green Synthesis of Silver Nanoparticles Using *Lysiloma acapulcensis* Exhibit High-Antimicrobial Activity. *Scientific Reports*, **10**, Article No. 12805. https://doi.org/10.1038/s41598-020-69606-7

[32] Balavijayalakshmi, J. and Ramalakshmi, V. (2017) *Carica papaya* Peel Mediated Synthesis of Silver Nanoparticles and Its Antibacterial Activity against Human Pathogens. *Journal of Applied Research and Technology*, **15**, 413-422. https://doi.org/10.1016/j.jart.2017.03.010

[33] Veerasamy, R., Xin, T.Z., Gunasagaran, S., Xiang, T.F.W., Yang, E.F.C., Jeyakumar, N. and Dhanaraj, S.A. (2011) Biosynthesis of Silver Nanoparticles Using Mangosteen Leaf Extract and Evaluation of Their Antimicrobial Activities. *Journal of Saudi Chemical Society*, **15**, 113-120. https://doi.org/10.1016/j.jscs.2010.06.004

[34] Srirangam, G.M. and Parameswara Rao, K. (2017) Synthesis and Charcterization of Silver Nanoparticles from the Leaf Extract of *Malachra capitata* (L.). *Rasayan Journal of Chemistry*, **10**, 46-53. https://doi.org/10.7324/RJC.2017.1011548

[35] Vishwasrao, C., Momin, B. and Ananthanarayan, L. (2019) Green Synthesis of Silver Nanoparticles Using Sapota Fruit Waste and Evaluation of Their Antimicrobial Activity. *Waste and Biomass Valorization*, **10**, 2353-2363. https://doi.org/10.1007/s12649-018-0230-0

[36] Ren, Y., Yang, H., Wang, T. and Wang, C. (2019) Bio-Synthesis of Silver Nanoparticles with Antibacterial Activity. *Materials Chemistry and Physics*, **235**, Article ID: 121746. https://doi.org/10.1016/j.matchemphys.2019.121746

[37] Asimuddin, M., Shaik, M.R., Fathima, N., Afreen, M.S., Adil, S.F., Siddiqui, M.R.H., Jamil, K. and Khan, M. (2020) Study of Antibacterial Properties of Ziziphus Mauritiana Based Green Synthesized Silver Nanoparticles against Various Bacterial Strains. *Sustainability*, **12**, Article No. 1484. https://doi.org/10.3390/su12041484

[38] Sun, L., Lv, P.C., Yin, Y.C., Li, H.N. and Wang, F. (2018) Green Synthesis of Silver Nanoparticles Using Wolfberry Fruits Extract and Their Photocatalytic Performance. *IOP Conference Series*: *Materials Science and Engineering*, **292**, Article ID: 012017. https://doi.org/10.1088/1757-899X/292/1/012017

[39] Kumar, K., Kumar, D. and Punathil, R.R. (2018) Green Synthesis of Silver Nanoparticles Using *Hydnocarpus pentandra* Leaf Extract: *In-Vitro* Cyto-Toxicity Studies against MCF-7 Cell Line. *Journal of Young Pharmacists*, **10**, 16-19. https://doi.org/10.5530/jyp.2018.10.5

[40] Vanaja, M., Gnanajobitha, G., Paulkumar, K., Rajeshkumar, S., Malarkodi, C. and Annadurai, G. (2013) Phytosynthesis of Silver Nanoparticles by *Cissus quadrangularis*: Influence of Physicochemical Factors. *Journal of Nanostructure Chemistry*, **3**, Article No. 17. https://doi.org/10.1186/2193-8865-3-17

[41] Kaabipour, S. and Hemmati, S. (2021) A Review on the Green and Sustainable Synthesis of Silver Nanoparticles and One-Dimensional Silver Nanostructures. *Beilstein Journal of Nanotechnology*, **12**, 102-136. https://doi.org/10.3762/bjnano.12.9

[42] Akhlaghi, S.P., Peng, B., Yao, Z. and Tam, K.C. (2013) Ustainable Nanomaterials Derived from Polysaccharides and Amphiphilic Compounds. *Soft Matter*, **9**, 7905-7918. https://doi.org/10.1039/c3sm50358e

[43] Duan, H., Wang, D. and Li, Y. (2015) Green Chemistry for Nanoparticle Synthesis. *Chemical Society Review*, **44**, 5778-5792. https://doi.org/10.1039/C4CS00363B

[44] Sokrates, G. (2004) Infrared and Raman Characteristic Group Frequencies: Tables and Charts. 3rd Edition, John Wiley & Sons Ltd., Chichester.

[45] Li, X., Tang, Y., Xuan, Z., Liu, Y. (2007) Study on the Preparation of Orange Peel Cellulose Adsorbents and Biosorption of Cd^{2+} from Aqueous Solution. *Separation and Purification Technology*, **55**, 69-75. https://doi.org/10.1016/j.seppur.2006.10.025

[46] Singh, P., Pandit, S., Beshay, M., Mokkapati, V.R.S.S., Garnaes, J., Olsson, M.E., Sultan, A., Mackevica, Mateiu, A.R.V., Lütken, H., Daugaard, A.E., Baun, A. and Mijakovic, I. (2018) Anti-Biofilm Effects of Gold and Silver Nanoparticles Synthesized by the *Rhodiola rosea* Rhizome Extracts. *Artificial Cells*, *Nanomedicine Biotechnology*, **46**, S886-S899. https://doi.org/10.1080/21691401.2018.1518909

[47] Dong, C., Cao, C., Zhang, X., Zhan, Y., Wang, X., Yang, X., Zhou, K., Xiao, X. and Yuan, B. (2017) Wolfberry Fruit (*Lycium barbarum*) Extract Mediated Novel Route for the Green Synthesis of Silver Nanoparticles. *Optik* (*Stuttg*), **130**, 162-170. https://doi.org/10.1016/j.ijleo.2016.11.010

[48] Zafar, S. and Zafar, A. (2019) Biosynthesis and Characterization of Silver Nanoparticles Using *Phoenix dactylifera* Fruits Extract and Their *in Vitro* Antimicrobial and Cytotoxic Effects. *The Open Biotechnology Journal*, **13**, 37-46. https://doi.org/10.2174/1874070701913010037

[49] Philip, D. (2010) Green Synthesis of Gold and Silver Nanoparticles Using *Hibiscus rosa* Sinensis. *Physica E*: *Low-Dimensional Systems and Nanostructures*, **42**,

1417-1424. https://doi.org/10.1016/j.physe.2009.11.081

[50] Rojas-Andrade, M., Cho, A.T., Hu, P., Lee, S.J., Deming, C.P., Sweeney, S.W., Saltikov, C. and Chen, S. (2015) Enhanced Antimicrobial Activity with Faceted Silver Nanostructures. *Journal of Materiel Science*, **50**, 2849-2858. https://doi.org/10.1007/s10853-015-8847-x

[51] Gomathi, M., Rajkumar, P.V., Prakasam, A. and Ravichandran, K. (2017) Green Synthesis of Silver Nanoparticles Using *Datura stramonium* Leaf Extract and Assessment of Their Antibacterial Activity. *Resource-Efficient Technologies*, **3**, 280-284. https://doi.org/10.1016/j.reffit.2016.12.005

[52] Raja, S., Ramesh, V. and Thivaharan, V. (2017) Green Biosynthesis of Silver Nanoparticles Using *Calliandra haematocephala* Leaf Extract, Their Antibacterial Activity and Hydrogen Peroxide Sensing Capability. *Arabian Journal of Chemistry*, **10**, 253-261. https://doi.org/10.1016/j.arabjc.2015.06.023

[53] Kora, A.J. and Arunachalam, J. (2012) Green Fabrication of Silver Nanoparticles by Gum Tragacanth (Astragalus Gummifer): A Dual Functional Reductant and Stabilizer. *Journal of Nanomaterials*, **2012**, Article ID: 869765. https://doi.org/10.1155/2012/869765

[54] Song, J.Y. and Kim, B.S. (2009) Rapid Biological Synthesis of Silver Nanoparticles Using Plant Leaf Extracts. *Bioprocess and Biosystems Engineering*, **32**, 79-84. https://doi.org/10.1007/s00449-008-0224-6

[55] Shameli, K., Mansor Bin Ahmad, M., Mohsen, Z., Yunis, W.Z., Ibrahim, N.A. and Rustaiyan, A. (2011) Synthesis of Silver Nanoparticles in Montmorillonite and Their Antibacterial Behavior. *International Journal of Nanomedicine*, **6**, 581-590. https://doi.org/10.2147/IJN.S17112

[56] Zargar, M., Hamid, A.A., Bakar, F.A., Shamsudin, M.N., Shameli, K., Jahanshiri, F. and Farahani, F. (2011) Green Synthesis and Antibacterial Effect of Silver Nanoparticles Using *Vitex negundo* L. *Molecules*, **16**, 6667-6676. https://doi.org/10.3390/molecules16086667

[57] Bagherzade, G., Tavakoli, M.M. and Namaei, M.H. (2017) Green Synthesis of Silver Nanoparticles Using Aqueous Extract of Saffron (*Crocus sativus* L.) Wastages and Its Antibacterial Activity against Six Bacteria. *Asian Pacific Journal of Tropical Biomedicine*, **7**, 227-233. https://doi.org/10.1016/j.apjtb.2016.12.014

[58] Shankar, S.S., Rai, A., Ahmad, A. and Sastry, M.J. (2004) Rapid Synthesis of Au, Ag, and Bimetallic Au Core-Ag Shell Nanoparticles Using Neem (*Azadirachta indica*) Leaf Broth. *Journal of Colloid and Interface Science*, **275**, 496-502. https://doi.org/10.1016/j.jcis.2004.03.003

[59] Kaviya, S., Santhanalakshmi, J., Viswanathan, B., Muthumary, J. and Srinivasan, K. (2011) Biosynthesis of Silver Nanoparticles Using Citrus Sinensis Peel Extract and Its Antibacterial Activity. *Spectrochimica Acta Part A*: *Molecular and Biomolecular Spectroscopy*, **79**, 594-598. https://doi.org/10.1016/j.saa.2011.03.040

[60] Jyoti, K., Baunthiyal, M. and Singh, A. (2016) Characterization of Silver Nanoparticles Synthesized Using *Urtica dioica* Linn. Leaves and Their Synergistic Effects with Antibiotics. *Journal of Radiation Research and Applied Sciences*, **9**, 217-227. https://doi.org/10.1016/j.jrras.2015.10.002

[61] Krishnaraj, C., Jagan, E.G., Rajasekar, S., Selvakumar, P., Kalaichelvan, P.T. and Mohan, N. (2010) Synthesis of Silver Nanoparticles Using *Acalypha indica* Leaf Extracts and Its Antibacterial Activity against Water Borne Pathogens. *Colloids Surfaces B Biointerfaces*, **76**, 50-56. https://doi.org/10.1016/j.colsurfb.2009.10.008

[62] Lakshmanan, G., Sathiyaseelan, A., Kalaichelvan, P.T. and Murugesan, K. (2018)

Plant-Mediated Synthesis of Silver Nanoparticles Using Fruit Extract of *Cleome viscosa* L.: Assessment of Their Antibacterial and Anticancer Activity. *Karbala International Journal of Modern Science*, **4**, 61-68. https://doi.org/10.1016/j.kijoms.2017.10.007

[63] Numan, A., Ahmed, M., Galil, M., Al-Qubati, M., Raweh, A. and Helmi, E. (2022) Bio-Fabrication of Silver Nanoparticles Using *Catha edulis* Extract: Procedure Optimization and Antimicrobial Efficacy Encountering Antibiotic-Resistant Pathogens. *Advances in Nanoparticles*, **11**, 31-54. https://doi.org/10.4236/anp.2022.112004

[64] Allec, N., Choi, M., Yesupriya, N., Szychowski, B., White, M.R., Kann, M.G., Garcin, E.D., Daniel, M. and Badano, A. (2015) Small-Angle X-Ray Scattering Method to Characterize Molecular Interactions: Proof of Concept. *Scientific Reports*, **5**, Article No. 12085. https://doi.org/10.1038/srep12085

[65] Feleni, U., Sidwaba, U., Makelane, H. and Iwuoha, E. (2019) Core-Shell Palladium Telluride Quantum Dot-Hemethiolate Cytochrome Based Biosensor for Detecting Indinavir Drug. *Journal of Nanoscience and Nanotechnology*, **19**, 7974-7981. https://doi.org/10.1166/jnn.2019.16866

[66] Plowman, B.J., Sidhureddy, B., Sokolov, S.V., Young, N.P., Chen, A. and Compton, R.G. (2016) Electrochemical Behavior of Gold-Silver Alloy Nanoparticles. *ChemElectroChem*, **3**, 1039-1043. https://doi.org/10.1002/celc.201600212

[67] Lima Filho, M.M.S., Correa, A.A., Silva, F.D.C., Carvalho, F.A.O., Mascaro, L.H. and Oliveira, T.M.B.F. (2019) A Glassy Carbon Electrode Modified with Silver Nanoparticles and Functionalized Multi-Walled Carbon Nanotubes for Voltammetric Determination of the Illicit Growth Promoter Dienestrol in Animal Urine. *Microchimica Acta*, **186**, Article No. 525. https://doi.org/10.1007/s00604-019-3645-9

[68] Khan, I., Pandit, U.J., Wankar, S., Das, R. and Limaye, S.N. (2017) Fabrication of Electrochemical Nanosensor Based on Polyaniline Film-Coated AgNP-MWCNT-Modified GCE and Its Application for Trace Analysis of Fenitrothion. *Ionics* (*Kiel*), **23**, 1293-1308. https://doi.org/10.1007/s11581-016-1939-z

[69] Raj, V., Vijayan, A.N. and Joseph, K. (2015) Cysteine Capped Gold Nanoparticles for Naked Eye Detection of *E. coli* Bacteria in UTI Patients. *Sensors and Bio-Sensing Research*, **5**, 33-36. https://doi.org/10.1016/j.sbsr.2015.05.004

[70] Sepunaru, L., Tschulik, K., Batchelor-McAuley, C., Gavish, R. and Compton, R.G. (2015) Electrochemical Detection of Single *E. coli* Bacteria Labeled with Silver Nanoparticles. *Biomaterials Science*, **3**, 816-820. https://doi.org/10.1039/C5BM00114E

[71] Boken, J., Dalela S., Sharma, C.K. and Kumar, D. (2013) Detection of Pathogenic *Escherichia coli* (*E. coli*) Using Robust Silver and Gold Nanoparticles. *Journal of Chemical Engineering & Process Technology*, **4**, Article ID: 1000175.

[72] Article, R. (2011) Methods for the Determination of Limit of Detection and Limit of Quantitation of the Analytical Methods. *Chronicles of Young Scientists*, **2**, 21-25. https://doi.org/10.4103/2229-5186.79345

[73] Armbruster, D.A., Tillman, M.D. and Hubbs, L. (1994) Limit of Detection (LOD)/Limit of Quantitation (LOQ): Comparison of the Empirical and the Statistical Methods Exemplified with GC-MS Assays of Abused Drugs. *Clinical Chemistry*, **40**, 1233-1238. https://doi.org/10.1093/clinchem/40.7.1233

[74] Yaghubi, F. and Zeinoddini, M. (2020) Design of Localized Surface Plasmon Resonance (LSPR) Biosensor for Immunodiagnostic of *E. coli* O157:H7 Using Gold Nanoparticles Conjugated to the Chicken Antibody. *Plasmonics*, **15**, 1481-1487.

https://doi.org/10.1007/s11468-020-01162-2

[75] Su, H., Ma, Q., Shang, K., Liu, T., Yin, H. and Ai, S. (2012) Gold Nanoparticles as Colorimetric Sensor: A Case Study on *E. coli* O157:H7 as a Model for Gram-Negative Bacteria. *Sensors Actuators*, *B Chemical*, **161**, 298-303. https://doi.org/10.1016/j.snb.2011.10.035

[76] Meeusen, Alocilja, E.C. and Ryser, E. (2001) Use of Biosensor for Pathogen Monitoring in the Pork Production Chain. American Society of Agricultural and Biological Engineers, St. Joseph, Paper No. 017031.

[77] Elkind, J.L., Stimpson, D.I., Strong, A.A., Bartholomew, D.U. and Melendez, J.L. (1999) Integrated Analytical Sensors: The Use of the TISPR-1 as a Biosensor. *Sensors and Actuators B*: *Chemical*, **54**, 182-190. https://doi.org/10.1016/S0925-4005(98)00336-0

[78] Wang, S., Xie, J., Jiang, M., Chang, K., Chen, R., Ma, L., Zhu, J., Guo, Q., Sun, H. and Hu, J. (2016) The Development of a Portable SPR Bioanalyzer for Sensitive Detection of *Escherichia coli* O157:H7. *Sensors*, **16**, Article No. 1856. https://doi.org/10.3390/s16111856

[79] Wang, C. and Irudayaraj, J. (2008) Gold Nanorod Probes for the Detection of Multiple Pathogens. *Nano Micro Small Communication*, **4**, 2204-2208. https://doi.org/10.1002/smll.200800309

[80] Cui, M., Chang, H., Zhong, Y., Wang, M., Wu, T., Hu, X., Xu, Z.J. and Xu, C. (2018) Detection of Bacteria in Water with β-Galactosidase-Coated Magnetic Nanoparticles. *SLAS Technology*: *Translating Life Sciences Innovation*, **23**, 624-630. https://doi.org/10.1177/2472630318773407

[81] Zhou, C., Zou, H., Li, M., Sun, C., Ren, D. and Li, Y. (2018) Fiber Optic Surface Plasmon Resonance Sensor for Detection of *E. coli* O157:H7 Based on Antimicrobial Peptides and AgNPs-rGO. *Biosensors and Bioelectronics*, **117**, 347-353. https://doi.org/10.1016/j.bios.2018.06.005

[82] Panhwar, S., Hassan, S.S., Mahar, R.B., Carlson, K., Rajput, M. and Talpur, M.Y. (2019) Highly Sensitive and Selective Electrochemical Sensor for Detection of *Escherichia coli* by Using L-Cysteine Functionalized Iron Nanoparticles. *Journal of Electrochemical Society*, **166**, B227-B235. https://doi.org/10.1149/2.0691904jes

[83] Ho, J.S. and Toh, C. (2013) A Rapid Low Power Ultra-Violet Light-Assisted Bacterial Sensor for Coliform Determination. *American Journal of Analytical Chemistry*, **4**, 1-8. https://doi.org/10.4236/ajac.2013.410A1001

[84] Stoimenov, P.K., Klinger, R.L., Marchin, G.L. and Klabunde, K.J. (2002) Metal Oxide Nanoparticles as Bactericidal Agents. *Langmuir*, **18**, 6679-6686. https://doi.org/10.1021/la0202374

[85] Armbruster, D.A. and Pry, T. (2008) Limit of Blank, Limit of Detection and Limit of Quantitation. *The Clinical Biochemist Reviews*, **29**, S49-S52.

[86] Cimafonte, M., Fulgione, A., Gaglione, R., Papaianni, M., Capparelli, R., Arciello, A., Censi, S.B., Borriello, G., Velotta, R. and Della Ventura, B. (2020) Screen Printed Based Impedimetric Immunosensor for Rapid Detection of *Escherichia coli* in Drinking Water. *Sensors* (*Switzerland*), **20**, Article No. 274. https://doi.org/10.3390/s20010274

[87] Hassan, A.R.H.A.A., de la Escosura-Muñiz, A. and Merkoçi, A. (2015) Highly Sensitive and Rapid Determination of *Escherichia coli* O157:H7 in Minced Beef and Water Using Electrocatalytic Gold Nanoparticle Tags. *Biosensors and Bioelectronics*, **67**, 511-515. https://doi.org/10.1016/j.bios.2014.09.019

[88] Pangajam, A., Theyagarajan, K. and Dinakaran, K. (2019) Highly Sensitive Electrochemical Detection of *E. coli* O157:H7 Using Conductive Carbon Dot/ZnO Nanorod/PANI Composite Electrode. *Sensors and Bio-Sensing Research*, **29**, Article ID: 100317. https://doi.org/10.1016/j.sbsr.2019.100317

[89] Cheng, Y., Liu, Y., Huang, J., Feng, Z., Xian, Y., Wu, Z., Zhang, W. and Jin, L. (2008) Platinum Nanoparticles Modified Electrode for Rapid Electrochemical Detection of *Escherichia coli*. *Chinese Journal of Chemistry*, **26**, 302-306. https://doi.org/10.1002/cjoc.200890059

[90] Tarditto, L.V., Arévalo, F.J., Zon, M.A., Ovando, H.G., Vettorazzi, N.R. and Fernández, H. (2016) Electrochemical Sensor for the Determination of Enterotoxigenic *Escherichia coli* in Swine Feces Using Glassy Carbon Electrodes Modified with Multi-Walled Carbon Nanotubes. *Microchemical Journal*, **127**, 220-225. https://doi.org/10.1016/j.microc.2016.03.011